Forensic Analysis of Retaining Wall Failure

P. S. Aravind and Neerad Mohan

1 Introduction

Forensic investigations involve field and laboratory tests apart from the collection of all available data as well as distress measurements. The test parameters and design assumptions in the forensic analysis will have to be representative of the actual conditions encountered at the site [11]. It often includes a collection of data, characterization of distress, development of failure hypothesis, diagnostic tests, and back analysis [12]. In the present case, forensic geotechnical analysis of the gravity retaining wall is performed to determine the possible causes of the failure of the wall.

1.1 Description of Gravity Wall

The gravity wall is located in Muringoor village, Chalakudy, Trichur district, India, on the banks of the Chalakudy river. It is situated adjacent to Bridge no. 132 of Indian railways (Fig. 1). The 15 m × 1.5 m × 3.0 m wall is a non-monolithic construction joined to the abutment of the bridge by ashlar masonry. The base of the retaining wall is located at a depth of 7.92 m below the track level. The site has a history of slope stability problems on both east and west sides. When a major crack was observed, the tilt is kept under observation, and measurements are taken. Gradually, the tilting increased, and the entire 15 m long retaining wall collapsed into the river (Fig. 2). Unsatisfactory packing of ashlar masonry, insufficient drainage facility, and few dowel bars could be seen. The retaining wall provided is a rigid one having been constructed in a continuous length. During the inspection, it is observed that the soil

P. S. Aravind · N. Mohan (✉)
Thejus Engineering College, Trichur, Kerala, India

C. N. V. Satyanarayana Reddy et al. (eds.), *Dynamics of Soil and Modelling of Geotechnical Problems*, Lecture Notes in Civil Engineering 186,
https://doi.org/10.1007/978-981-16-5605-7_1

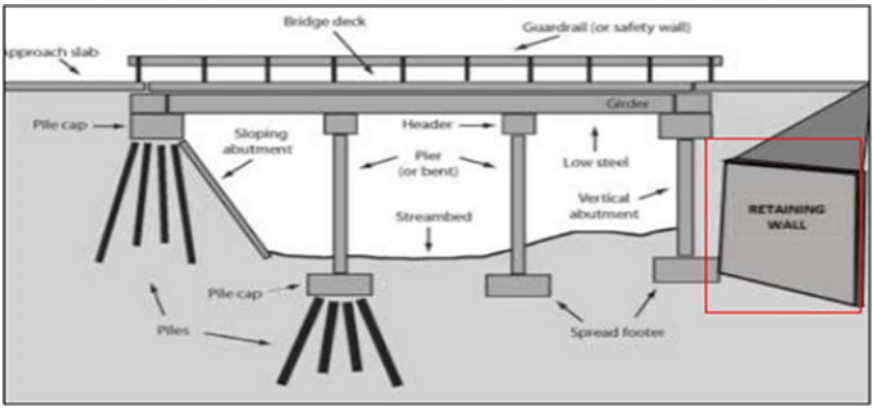

Fig. 1 Retaining wall located adjacent to the bridge abutment

Fig. 2 Collapsed retaining wall

becomes very slushy having very little shear strength after encountering water. Weep holes are provided on the retaining wall but are found to be clogged.

2 Characterization of Distress

The distresses that are observed in the field are in the form of lateral movements and vertical settlements. The abutment wall of bridge no. 132 is taken as the reference point (0, 0) for the measurement of the horizontal lateral displacement of the gravity wall. Maximum lateral displacement of 90 mm is observed as shown in Fig. 3. It also shows the vertical settlement of the wall measured to track level. From field

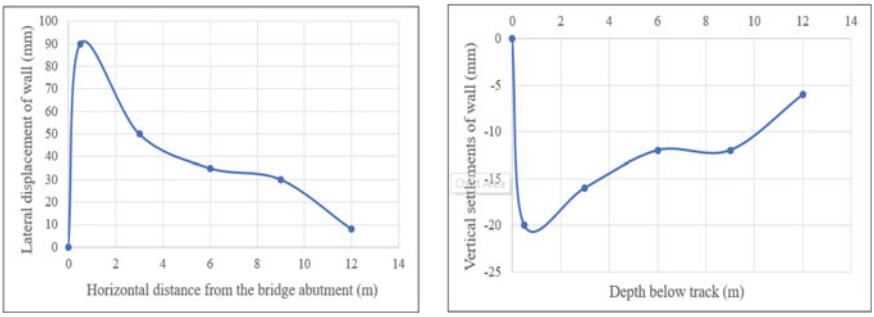

Fig. 3 Collapsed retaining wall

measurements, a maximum vertical displacement of 20 mm is observed at 0.5 m from the bridge abutment. The maximum distress due to lateral movement and vertical settlements is found in the region where the retaining wall joins the bridge abutment. Figure 4 shows the magnitude of distress patterns of lateral deformation. Figure 5 shows visual cracks (more than 60 mm wide) on the inclined slope due to excessive vertical settlement of both backfill and foundation soil beneath the gravity wall. The measured values are compared with deformation values obtained from both displacement analysis and numerical analysis.

Fig. 4 Laterally displaced retaining wall

Fig. 5 Cracks due to vertical settlement

3 Collection and Interpretation of Test Data

A standard penetration test is done to determine geotechnical properties, relative density, and penetration resistance of soil layers. Trial pit-1 excavated at 2.69 m below the track level consists of backfill soil and trial pit-2 located at 7.92 m below the track level consists of natural foundation soil at the site. The trial pit soil samples are used to determine the basic and engineering properties of the soil. Shear strength properties are determined by the undrained unconsolidated triaxial test, and the coefficient of permeability is determined by the constant head permeability test. Tables 1, 2, and 3 present the geotechnical properties of soil samples.

3.1 Soil Profile

Backfill is clayey SAND and it is present until a depth of 7.5 m. The zone's geology features poorly graded SAND from 7.5 to 19.5 m. Underneath them, the lower stratum

Table 1 Properties of trial pit soil samples

Location	Natural moisture content (%)	Specific gravity (G)	Gravel (%)	Sand (%)	Fines (%)	LL (%)	PL (%)	PI
T.P 1	19	2.66	5	57	38	33	16	17
T.P 2	10	2.65	0	70	30	41	N.D	N.D

Table 2 Permeability characteristics of soil samples

Soil	Coefficient of permeability (mm/s)	Drainage property	USBR Classification
SC	1×10^{-4}	Poor	Semi pervious
SP	1.59×10^{-3}	Fair	Pervious
SM	4.14×10^{-2}	Good	Pervious

Table 3 Engineering properties of soil

Location	T.P.1	T.P.2
Cohesion (kPa)	5	0
Frictional Angle (°)	29	30
Young's Modulus (kPa)	7500	7000
Shear Modulus (kPa)	2885	2692
MDD (kPa)	18.4	18.0
OMC (%)	24.0	12.5
Bulk density (kN/m^3)	17.6	17.7
Dry density (kN/m^3)	14.7	16.4
Saturated density (kN/m^3)	19.2	20.3

consists of silty SAND till a depth of 22.5 m beyond which bedrock is present. The rock samples obtained are Charnockite Gneiss and Granite, a common type of hard geological rock found in the Chalakudi district. Relative density values obtained show the presence of loose to medium dense followed by very dense soil strata. The SPT test results show that the site has weak soil at shallow depth. It also reveals that proper compaction is not provided before construction. The RQD of the rock varies from 70 to 80%. The rock samples show good recovery indicating the presence of firm good bedrock strata at 22.5 mt from the ground level. The groundwater level is encountered at 9.52 m with a dip meter. The water level in the river rises during the monsoon season when the nearby dam shutters are opened. As a result, the water level rises to 6 m, and the gravity wall is partially submerged underwater.

4 Field Instrumentation for Measurement of Ground Vibration

MEMS-based triaxial accelerometer ADXL 335 is used for the measurement of the train-induced ground vibrations. Accelerometers are sensors that usually detect accelerations by utilizing inertial force. The ADXL 335 circuit performs signal measurement and amplification to obtain a low amplitude signal. Here, the amplified signal is collected by Arduino micro-controller, and these acquired data are sent via a serial communication protocol to third-party devices, i.e. the laptop. The extension of the railway line was considered for the study and the numerical model has a length of 11 m. An area considered incorporates the railway track, the bridge abutment, the backfill slope, and the retaining wall. The site has a stepped arrangement post slope failure. The entire site is divided into gridlines. Due to the stepped arrangement of the site, the gridlines 1, 2, and 3 are normal to the track and at certain points located at different levels below w.r.t the ground/track level. Gridlines A, B, and C are located at distances of 1.5, 6.5, and 11.5 m from the edge of the railway track. It intersects the gridlines 1, 2, and 3 at A1, A2, A3, B1, B2, B3, C1, C2, and C3. Points B3 and

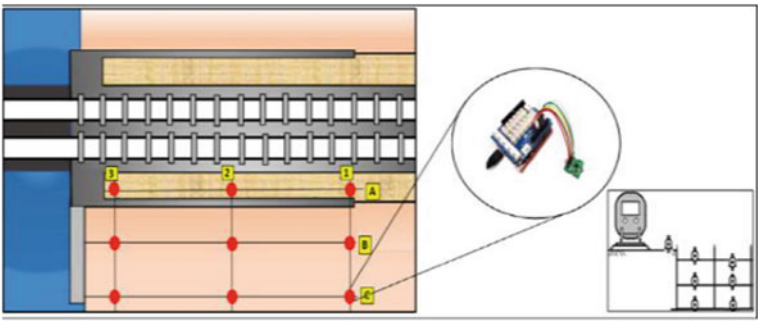

Fig. 6 Field Instrumentation setup

C3 are located closest to the collapsed retaining wall. These points of intersection of gridlines give the measurement points where the triaxial accelerometers are placed. The arrangement is orientated in both the longitudinal and transverse directions of the vibration source and the proximity of the railway track and collapsed gravity wall. The following schematic diagram Fig. 6 shows the instrumentation setup.

5 Time-and Frequency-Domain Parameters

The ground vibration data obtained during the movement of the train are acquired and processed. The typical time-histories of vertical, longitudinal, and lateral acceleration of vibration produced in the soil during train movement for locations B2 and C1 are shown in Figs. 7 and 8. The maximum peak vertical acceleration is about 0.17 g which occurs at a distance of 1.5 m from the track lane.

The time-domain parameters are transformed into frequency-domain parameters using the Fourier transform technique (Fig. 9). Acceleration signals are processed by doing numerical integration to get corresponding peak particle velocity. A Digital filter (IIR—infinite impulse response filter) was used to eliminate noise. Peak ground acceleration, peak particle velocity, frequency, and displacement are determined. The results of vibration analysis (Table 4) are used to determine the influence of train-

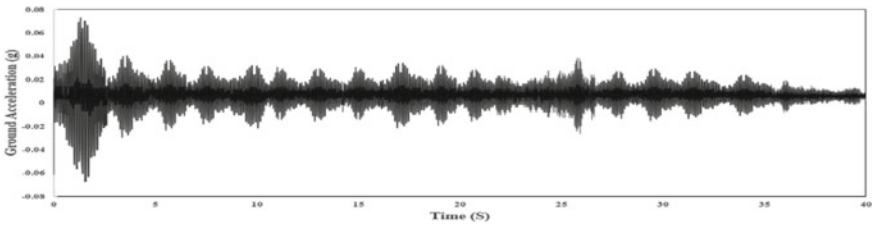

Fig. 7 Acceleration versus time graph for location B2

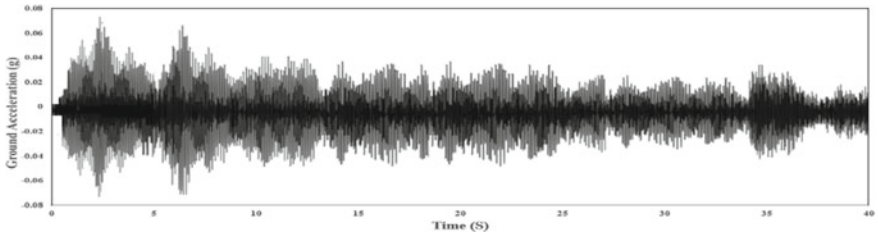

Fig. 8 Acceleration versus time graph for location C1

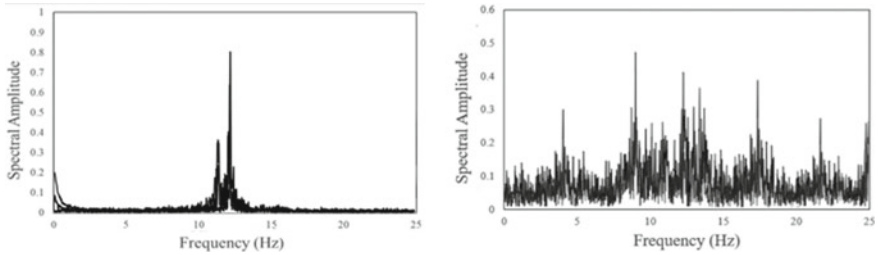

Fig. 9 Spectral amplitude versus frequency

induced ground vibration on producing resonance conditions in the soil and related liquefaction.

6 Characteristics of the Soil Layers

For the estimation of eigenfrequencies of subsoils, a horizontal layered ground is considered, and the frequency is dependent on two factors in the soil, the shear wave velocity and thickness of the subsoil. The subsoils expected eigenfrequency is calculated as follows:

$$f_o = \frac{V_s}{4H} = \sqrt{\frac{G/\gamma}{4H}}$$

H: Total layer thickness of soil layers.
G: Shear modulus of the soil layer.
γ: Density of the soil layer.
V_s: Shear wave velocity.

Using the free-vibration decay method [2], the damping ratio ξ (fraction of critical damping) from the ratio of two peaks a_n and a_{n+m} over m consecutive cycles in the selected area of the acceleration-time curve history is determined with the following equation

Table 4 Ground vibration parameters

Location	Distance from source			Ground acceleration			Frequency	Peak particle velocity
	Damping Ratio	Depth/Level below track (m)	X_{max} Longitudinal (g)	Y_{max} Lateral (g)	Z_{max} Vertical (g)	Peak ground Acceleration (g)	Dominant Frequency (HZ)	SSRS (mm/s)
A1	0.3	0	0.12	0.13	0.17	0.17	22	15.43
A2	0.3	0	0.14	0.12	0.15	0.15	18	15.89
A3	1.5	0	0.13	0.08	0.11	0.13	14	11.90
B1	6.5	1	0.10	0.05	0.08	0.10	17	7.91
B2	6.5	4	0.01	0.07	0.02	0.07	16	5.47
B3	6.5	8	0.02	0.03	0.01	0.03	12	2.59
C1	11.5	2	0.07	0.06	0.03	0.07	13	6.19
C2	11.5	4	0.06	0.06	0.03	0.06	13	5.45
C3	11.5	8	0.03	0.02	0.02	0.03	9	2.40

$$\xi = \frac{\ln\left(\frac{a_n}{a_{n+m}}\right)}{2\pi m}$$

The attenuation coefficient α is used as a measure of the decrease in measured vibration with increasing distance from the track using the following [3] equation:

$$\alpha = \frac{-\ln\left[\frac{V_2}{V_1}\left(\frac{R_1}{R_2}\right)^{-0.5}\right]}{R_2 - R_1}$$

α is the attenuation coefficient (m^{-1}).
V_1 is the vibration velocity nearer to the source (mm/s).
V_2 is the vibration velocity further from the source (mm/s).
R_1 is the nearer distance to the source (m).
R_2 is the further distance to the source (m).

The saturated cohesionless soils are mostly affected by the vibrations. From attenuation values (Table 5), the foundation soil is classified as weak [1].

The natural frequencies of the wall are determined by Nandakumaran et. al solution for pure translation method and are presented in Table 6. It can be noticed from Table 6 that the measured eigenfrequency/dominant frequency of ground vibration is very close to the estimated/expected eigenfrequency for the foundation soil.

Table 5 Ground vibration parameters

Soil layer	Damping ratio	Attenuation coefficient 'α'	Soil characteristics
Soil layer 1 (Backfill 0–4 m)	0.3	0.0002	Competent
Soil layer 2 (Backfill 0–4 m)	0.3	0.002	Weak
Soil layer 3 (Foundation soil 7.5–19.5 m)	0.5	0.001	Weak

Table 6 Ground vibration parameters

System	Expected eigenfrequencies (Hz)	Measured eigenfrequencies (Hz)
Train	40–60	–
Backfill soil	1–10	13–17
Foundation soil	6–10	9–12
Retaining wall	4–9	2

7 Development of Failure Hypothesis

Assumptions are made regarding the possibility of the collapse of the retaining wall. To determine the cause of the collapse of the wall, the site conditions are selected to represent the 'worst possible' scenario, i.e. where it was considered that under the combination of high vibration levels induced by train, unfavorable soil, and backfill conditions along with various static and dynamic forces are acting on the wall are responsible for the collapse of the wall. The following failure hypothesis is developed such as high stresses induced due to ground vibrations, unfavorable soil conditions, the susceptibility of soil to undergo liquefaction, an increase in lateral thrust on the wall, and unscientific design and construction.

8 Back Analysis

The back analysis is conducted on the distressed retaining wall using vibrational analysis, conventional methods, and finite element analysis using PLAXIS 3D.

8.1 Vibrational Analysis

Ground-borne vibrations are generated by dynamic loads that induce energy into the soil and cause wave propagation in the ground [4, 5]. Liquefaction is defined as the transformation of granular material from a solid to a liquefied state because of increased pore water pressure and reduced effective stress [8]. Dynamic loads such as train-induced ground vibration can lead to resonance conditions in the soil which causes liquefaction in saturated cohesionless soils [7, 10]. The loose soil compacts and densifies due to the train-induced ground vibrations. Increased pore water pressure is induced by the tendency of granular materials to compact when subjected to cyclic shear deformations. Therefore, the ability of compaction of the soil is a factor that determines the liquefaction potential [10]. The change of state occurs mostly in loose to moderately dense granular soils with poor drainages, such as silty sands or sands and gravels capped by or containing seams of impermeable sediment. As liquefaction occurs, the soil stratum softens, allowing large cyclic deformations to occur [6]. In loose materials, the softening is also accompanied by a loss of shear strength that may lead to large shear deformations or even flow failure under moderate to high shear stresses, such as beneath a foundation or sloping ground. Resonance impact on soil leads material deterioration to occur followed by an increase of fine-grained material between larger particles causing degradation of shear modulus, shear strength, and bearing capacity which leads to settlements [7]. Loose soils also compact during liquefaction and reconsolidation, leading to differential settlement

and consequent structural damage. Liquefaction, through analysis, is confirmed. This would cause the subsoil to lose its bearing capacity which would lead to settlements.

Also, due to excessive rainfall and flood conditions frequently occurring, there will be a risk that the pore water pressure is built up in the soil which becomes high due to poor impermeable backfill and lack of proper drainage conditions. The possible consequence of this pore water pressure built up is the soil loses its bearing capacity and undergoes settlement. The low permeability backfill present also leads to water retention and adds up to the problem. In the project, the measurements of vibrations for soil layers and an analysis method focusing on the frequency content of the soil layer are performed, and the Eigenfrequencies/dominant frequency of the soil layer is determined. This measured highest amplitude peak for frequencies gives resonance frequencies/dominant frequency of the train-induced ground vibration for that soil layer. The values of the dominant frequency of the ground vibration give the resonance condition of different soil layers occuring. The expected Eigenfrequencies are obtained by empirical formulas. The expected eigenfrequencies are similar to the measured dominant frequencies, and the soil layer is said to undergo resonance at that frequency conditions which lead to liquefaction. Thus, an assessment of the dynamic loadings influences on various soil layers due to train-induced vibrations is performed. The vibrational analysis is a back analysis technique that is compared with the liquefaction resistance ratio which confirms the susceptibility of foundation soil to undergo liquefaction.

8.2 Conventional Analysis

In the conventional analysis, the seismic analysis of the retaining wall was performed to determine the various static and dynamic earth pressures acting on the wall. The design was performed for static condition and dynamic condition with zero and some allowable displacement using Coulomb's theory, the Mononobe-Okabe method, and the Richard-elms method, respectively. Hydrodynamic pore water pressure acting on the wall due to the river is determined by equations of Matzuo and O'Hara [9]. The displacement was determined for the wall for pure translation by the Nandakumaran et al. method. The dynamic bearing capacity was calculated by Richard et al. along with corresponding settlements. The section of the retaining wall was analyzed by stability check against sliding, overturning, and bearing capacity failure. Figure 10 shows forces acting on the gravity wall. Seismic analysis of retaining wall design is performed to determine the translation of the wall. The results of displacement analysis and settlement calculations which showed deformation in the form of translation and vertical settlements are presented. Using conventional methods, the stability of the retaining wall is checked for four prominent failure modes like overturning, sliding, and bearing capacity failure.

Table 7 shows the obtained values of earth pressure for the static and dynamic conditions with various methods. The lateral thrust in case 2 is more than case 1, which shows active lateral thrust increases when soil is saturated.

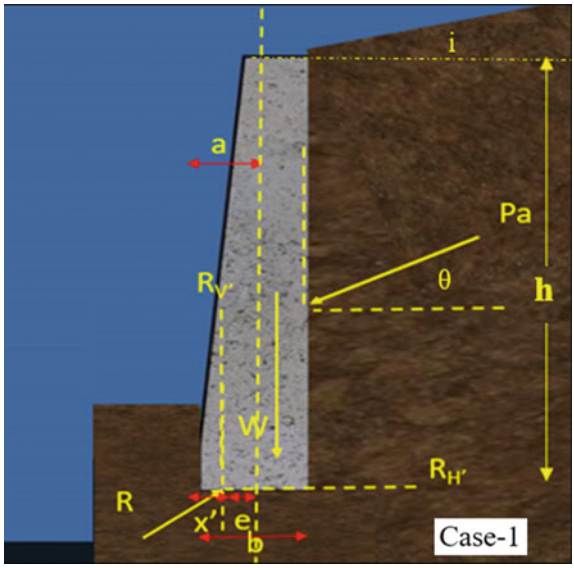

Fig. 10 Forces acting on gravity retaining wall

Table 7 Total lateral active thrust on the wall in static and dynamic conditions

Field condition	Specification	Method	Total Lateral active thrust on the wall, kN/m^2
Case 1–Field condition with dynamic active earth pressure acting on the wall	Static pressure acting on the gravity wall. Design based on force equilibrium	Coulomb theory	22.09
	Seismic pressure on gravity wall. Design based on seismic pressure	Mononobe-Okabe method	48.55
	Seismic displacement of gravity wall. Design based on allowable displacements	Richard-Elms method	34.77
Case 2–Saturated condition with dynamic active earth pressure and hydrodynamic loads acting on the wall	Static pressure acting on the gravity wall Design based on force equilibrium	Coulomb theory	27.67
	Seismic pressure on gravity wall. Design based on seismic pressure	Mononobe-Okabe method	56.54
	Seismic displacement of gravity wall. Design based on allowable displacements	Richard-Elms method	41.51

Table 8 Weight of wall under both static and dynamic conditions

Condition	Existing weight of wall (kN/m)	Safe weight of wall required (kN/m)	Remark
Static	150	124.64	Unsafe
Dynamic	150	150.69	Unsafe

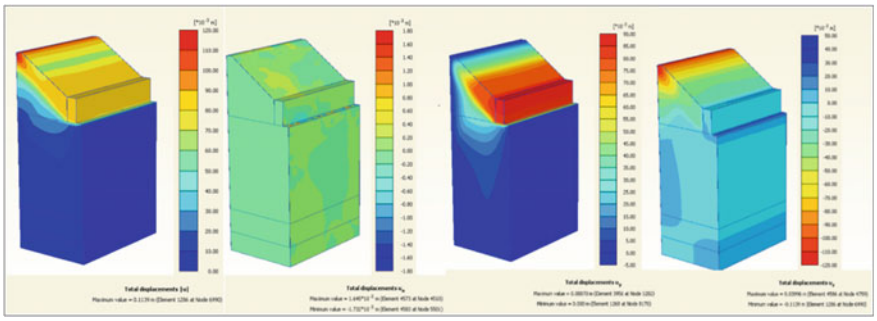

Fig. 11 Numerical analysis using PLAXIS 3D

Table 8 shows that the weight of the wall designed to resist movement due to static loads is quite high than required. Since the wall is founded on weak soil, it will not be able to bear the additional weight of the wall and collapse. Similarly, the weight of the wall provided to resist the movement due to dynamic loads is not sufficient. Hence, the wall is unsafe in both cases.

8.3 Numerical Analysis

The numerical analysis of the gravity retaining wall using FEM software Plaxis 3D is performed (Fig. 11). The deformations are obtained.

9 Comparison of Back Analysis Results

The foundation soil is loose and saturated. The results of conventional back analysis and numerical analysis are found to produce comparable results with the site deformations. The factor of safety obtained from conventional back analysis and numerical analysis is compared. The wall collapsed as a result of bearing capacity failure. Unscientific design and construction of the wall on weak soil led to this kind of failure. The soil present below the wall is already susceptible to liquefaction. The train-induced vibrations accelerated the liquefaction in the foundation soil

Table 9 Comparison of deformations

Method	Lateral displacement (mm)	Vertical displacement (mm)
Seismic displacement analysis and settlement calculation	100	28
Numerical analysis	80	30
Distress measurement at the site	90	20

Table 10 Comparison of results of back analysis

Conventional back analysis (by stability check)			
FS	Overturning	Sliding	Bearing capacity failure
	5.4	2.5	2.4
Numerical analysis using PLAXIS 3D			
Global FS	1		

and backfill. This led to the loss of bearing capacity of the soil and the wall underwent differential settlement leading to collapse. In addition to this, the presence of poor backfill material and lack of drainage led to water retention during rain and floods. The train-induced vibrations caused a rearrangement of the fine-sized particles, which increased the pore water pressure and effective stress decreased which resulted in liquefaction of the foundation soil. This induced additional lateral thrust on the wall resulting in its collapse. In Table 9, the deformations obtained from the site are compared with the conventional back analysis results and numerical PLAXIS 3D software results. The deformations conform with the numerical and conventional back analysis results. The factor of safety is obtained and the mechanism of failure of retaining wall design is presented (Table 10).

10 Conclusions

The vibrations were found to be very weak to cause any significant damage to the structure. The foundation soil is susceptible to liquefaction. The train-induced vibrations act as a trigger mechanism leading to liquefaction and differential settlement of foundation soil. The backfill soil has poor permeability which leads to water retention and exerts the additional lateral thrust on the wall. Stability checks performed show that the mechanism of failure is bearing capacity failure. The weight of the wall designed to resist movement due to static loads is quite high than required. Since the wall is founded on weak soil, it will not be able to bear the additional weight of the wall and undergo bearing capacity failure. The deformations obtained from conventional and numerical methods are compared with the deformations at the site. They are found to produce comparable results. A cantilever retaining wall on a pile foundation is the possible solution to the problem.

References

1. Amick H.: Frequency-dependent soil propagation model. Proc SPIE. 72–80. https://doi.org/10.1117/12.363836 (1999)
2. Chopra A..K.: Dynamics of Structures: Theory and Applications to Earthquake Engineering, Pearson Education Limited (2014)
4. Chouw, N., R. Le, G. Schmid: "Vibration transmitting behavior of the soil", Proc. of the Europ. Conf. on Struct. Dyn. (Eurodyn '90), Univ. of. Bochum, Germany, A.A. Balkema (1991)
3. Dowding C.H.: Construction Vibrations, 2nd Edition, Intl Society of Explosives (2000)
5. Hall L.: Simulations and analyses of train-induced ground vibrations in finite element models. Soil Dynamics and Earthquake Engineering, 23, 403–413 (2003). https://doi.org/10.1016/S0267-7261(02)00209-9.
6. Kramer, S.L.: Geotechnical Earthquake Engineering. Prentice-Hall, Upper Saddle River, New Jersey (1996)
7. Lichtberger, B.: Track Compendium, Eurail Press. Tetzlaff-Hestra GmbH & Co., Hamburg, Germany (2005)
8. Marcuson, W.F.: Definition of Terms Related to Liquefaction, Journal of Geotechnical Engineering Division, ASCE, 104(9), 1197–1200 (1978)
9. Matsuo, H., O'hara. S.: Dynamic pore water pressure acting on quay walls during earthquakes Proceeding of the Third WorkI Conference on Earthquake Engineering. I ol. 1, New Zealand pp. 130–140 (1965)
10. Richart, R.E., Hall, J.R, Woods, R.D.: Vibrations of Soils and Foundations, Prentice Hall Inc., New Jersey (1970)
11. Robert, D.: Forensic Geotechnical and Foundation Engineering. McGraw Hill Education (1997)
12. Sivakumar Babu, G.L. et al.: Forensic analysis of failure of retaining wall. In: 15th Asian Regional Conference on Soil Mechanics and Geotechnical Engineering, Japanese Geotechnical Society (2015)